CHAPTER THREE

Fluorescence cross-correlation spectroscopy of lipid-peptide interactions on supported lipid bilayers

Xiaosi Li, Xiaojun Shi, Megan J. Kaliszewski and Adam W. Smith*
Department of Chemistry, The University of Akron, 190 Buchtel Common, Akron, OH, 44325-3601, United States
*Corresponding author: E-mail: asmith5@uakron.edu

Contents

Abstract

Electrostatic interactions drive molecular assembly and organization in the plasma membrane. Specific protein-lipid interactions, however, are difficult to resolve. Here we report on a unique approach to investigate these interactions with time-resolved fluorescence spectroscopy. The experiments were performed on a model membrane system consisting of a supported lipid bilayer with an asymmetric distribution of PIP_2 in the upper leaflet of the bilayer. The bilayer also contained nickel-chelating lipids that bind to a histidine-tagged peptide of interest. Both the peptide and the lipid were labeled with orthogonal fluorescent probes, so that diffusion and binding

Advances in Biomembranes and Lipid Self-Assembly, Volume 29
ISSN 2451-9634
https://doi.org/10.1016/bs.abl.2019.01.005

could be measured with two-color, pulsed-interleaved excitation fluorescence cross-correlation spectroscopy (PIE-FCCS). Our PIE-FCCS data showed significant lipid-peptide cross-correlation between PIP_2 lipids and membrane-bound cationic peptides. Cross-correlation is a direct indication of lipid-peptide binding and complexation. Together with mobility data, we quantified the degree of binding, which offers new insight into this class of lipid-peptide interactions. Overall, this is the first report of lipid-peptide cross-correlation by FCCS, and provides a new route to quantifying the interactions between proteins and lipid membranes, a key interface in cell signaling.

1. Introduction

Anionic phospholipids are key components of the cell plasma membrane that can act as substrates for protein binding [1]. Phosphatidylinositol 4,5-bisphosphate (PIP_2) is an anionic lipid that plays an important role in the cytoplasmic leaflet of the plasma membrane [2]. PIP_2 is essential for a number of membrane-related phenomena, including signal transduction, regulation of endocytosis and exocytosis, ion channel function and enzyme activation [3–6]. Many of these processes are regulated through specific interactions between PIP_2 and peripheral membrane proteins [7,8]. For example, myristoylated alanine-rich C-kinase substrate (MARCKS) binds PIP_2 and can thereby modulate the number of available PIP_2 lipids in the plasma membrane [9]. The N-terminal hydrophobic myristoyl group of MARCKS inserts into the plasma membrane; the effector domain (ED), which carries positively charged amino acids, interacts directly with up to three PIP_2 lipids [2,9,10]. The binding of MARCKS to PIP_2-containing membranes has been studied using several techniques including EPR spectroscopy [11], NMR spectroscopy [12], and x-ray reflectivity [13]. However, these methods do not provide direct evidence that PIP_2 lipids form a stable complex with the MARCKS peptide. In this paper, we describe a novel assay that combines a model membrane system with PIE-FCCS to quantitatively analyze lipid-peptide binding. PIE-FCCS reports on the correlated diffusion of lipids and bound peptides, which is direct evidence they are bound together in a single diffusing complex.

Single color fluorescence correlation spectroscopy FCS is well-suited for measuring the lateral mobility of lipids and bound proteins/peptides [14]. By exploiting the intensity fluctuations caused by single fluorophores diffusing through the detection area, FCS can measure local concentrations and diffusion coefficients with quantitative accuracy [15]. A dual-color version of FCS, fluorescence cross-correlation spectroscopy (FCCS), resolves the

correlated diffusion of two species [16,17]. It has been used to study membrane protein-protein interactions by our lab and others [18,19]. In principle, FCCS could also be used to study interactions between membrane proteins and membrane lipids by labeling the proteins and lipids with spectrally distinguishable fluorescent probes [20]. To our knowledge, however, this type of lipid-protein cross-correlation experiment has not been reported. Here we used pulsed interleaved excitation fluorescence cross-correlation spectroscopy (PIE-FCCS) to measure the interaction between anionic lipids and cationic peptides. With pulsed interleaved excitation, the spectrally resolved photons are assigned to one of the two excitation pulses [21]. This allows for a more quantitative assessment of time-correlated events in a lipid-protein system.

In the experiments reported below, we investigated lipid-peptide binding in an asymmetric supported lipid bilayer (asy-SLB) developed in our lab [22]. Time-resolved fluorescence was used to measure the interaction between poly-basic peptides and PIP_2 lipids in asy-SLBs. The PIP_2 lipid was labeled with a BODIPY analogue in the acyl chain to leave the

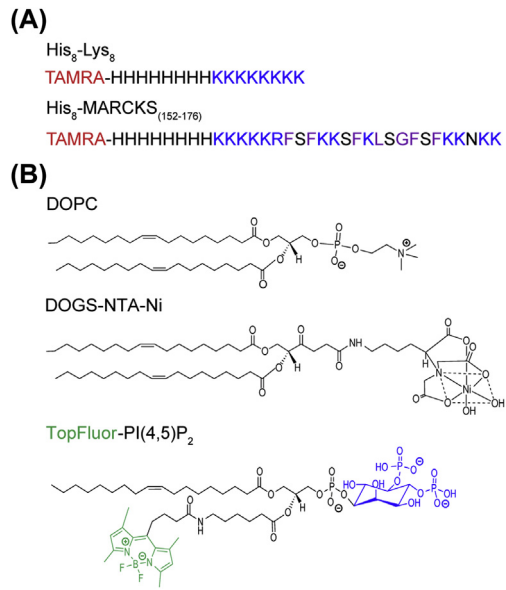

Figure 1 (A) The amino acid sequences of TAMRA-labeled His_8-Lys_8 and His_8-$MARCKS_{(152-176)}$ peptides are shown. *Blue text* indicates positively charged amino acid residues that can interact with negatively charged lipids. *Purple text* indicates amino acid residues with hydrophobic side chains that can penetrate the polar region of the lipid bilayer. (B) The chemical structures of DOPC, Ni^{2+}-NTA-DOGS and TopFluor-Labeled $PI(4,5)P_2$ lipids are shown.

headgroup unmodified (Fig. 1). Two cationic peptides were used as model systems in this study. The first peptide had eight lysine residues (His_8-Lys_8) and the second was the membrane proximal domain of MARCKS, His_8-$MARCKS_{(152-176)}$ (Fig. 1) [23]. The histidine residues were included to selectively bind nickel-chelating lipids, which anchored the peptide to the membrane so that we could directly probe the lateral, two-dimensional lipid-peptide interactions [24].

PIE-FCCS data revealed a significant level of cross-correlation between cationic peptides with anionic lipids. Specifically, we measured the experimentally determined relative value of cross-correlation (f_c) and lifetime, these data provide direct evidence of stable, electrostatically-driven lipid-peptide complexes. To analyze the data, we applied a two-component diffusion model, in which anionic lipids and cationic peptides assemble into slowly-diffusing lipid-peptide complexes [25]. Based on the two-component diffusion fits, we could resolve the extent of lipid-peptide binding, as well as an estimated of the size of the lipid-peptide complexes. Overall, our approach directly probes the extent of lipid-peptide complexation and provides a new way to study the dynamics of protein-lipid interactions.

2. Materials and methods

2.1 Lipid and reagents

1,2-Dioleoyl-sn-glycero-3-phosphatidylcholine (DOPC), 1,2-dioleoyl-sn-glycero-3-[(N-(5-amino-1-carboxypentyl)imino-diaceticacid) succinyl] (nickel salt) (DOGS-NTA-Ni^{2+}), 1,2-dioleoyl-sn-glycero-3-phospho-L-serine (DOPS), and 1-oleoyl-2-[6-[4(dipyrromethene boron difluoride) butanoyl]amino]hexanoyl-sn-glycero-3-phosphoinositol-4,5-bisphosphate (Top Fluor-$PI(4,5)P_2$), 1-palmitoyl-2-(dipyrromethene boron difluoride) undecanoyl-sn-glycero-3-phospho-L-serine (Top Fluor-PS) were purchased from Avanti Polar Lipids (Alabaster, AL).

Two working buffers were prepared, buffer A containing 0.8 mM sodium phosphate, 15.3 mM sodium chloride, 0.3 mM potassium chloride, 0.2 mM potassium phosphate, 100 nM EDTA (pH = 7.4). Buffer B containing 8 mM sodium phosphate, 153 mM sodium chloride, 3 mM potassium chloride, 2 mM potassium phosphate, 100 nM EDTA (pH = 7.4).

2.2 Peptide preparation

His_8-Lys_8 and His_8-$MARCKS_{(152-176)}$ peptides (sequences shown in Fig. 1) were obtained from Peptide 2.0, Inc and stored at -20 °C as arrived.

Fluorescent dyes tetramethylrhodamine (TAMRA) were added at N-terminus of the peptide for fluorescent probe labeling. The purity of the peptides was determined to be >95% by HPLC and MS. In order to disrupt peptide aggregation, the peptides were first dissolved in HFIP, after 2 h incubation, sonicated 30 min to remove aggregates, and then centrifuged at 14000 rpm for 30 min at −4 °C, 80% of top solution was collected and stored at −80 °C. The peptides were then dried with a freeze-dryer and used within 1 day [26].

2.3 Preparation of asymmetric supported lipid bilayers

Asymmetric SLB were prepared by vesicle-fusion as described in previous work [22]. Briefly, lipid mixture containing 96.5% mol% of DOPC, 3.5 mol% of DOGS-NTA-Ni^{2+} in chloroform were dried by rotational evaporation under vacuum. Deionized water was added to produce a final concentration of about 1 mg/mL lipid vesicle suspension. Next, by extruded lipid suspension with a 100 nm diameter porous membrane 15 times, the small unilamellar vesicles (SUVs) suspension were produced. The glass substrate was first sonicated with a detergent solution of 1:1 isopropanol and deionized water for 30 min, then sonicated again for 30 min in deionized water, and finally etched with piranha solution for 10 min, dried with nitrogen gas. 60 μL volume of SUVs suspension and 8 mM PBS mixture solution (1:1) were ruptured on the glass substrate, fusing into a symmetric lipid bilayer. The SLB were washed with 15 mL of deionized water and carefully exchanged to the buffer A. To form asy-SLB, SUVs containing 94.99 mol% of DOPC, 5 mol% of DOPS and 0.01 mol % of Top Fluor-$PI(4,5)P_2$ were added onto the SLB and incubated 10 min at room temperature before washing away unfused vesicles with 15 mL of buffer A. After washing, asy-SLB were incubated with 10 μL $NiCl_2$ in buffer A for 10 min and wash again.

2.4 FCS data analysis

Fluorescence correlation spectroscopy experiments were carried out with a customized inverted microscope (Nikon Eclipse Ti, Tokyo, Japan) [27]. Samples were excited by a supercontinuum white light fiber laser (SuperK NKT Photonics, Birkerod, Denmark) with a pulse rate of 9.7 MHz and a pulse duration of 5 ps. Two beams were selected to pass through the narrow-band filters. For blue excitation the light was filtered with a 488 nm bandpass filter (LL01-488-12.5, Semrock, Rochester, NY), and for green excitation the light was filtered with a 561 nm bandpass filter

(LL02-561-12.5, Semrock) before entering single mode fibers. The laser pulses were separated in time with a 15 m difference between the two optical fibers to achieve a 50 ns delay between the pulse arrival times. Fluorescence excitation and emission were collected through a 100X TIRF objective (NA 1.47 oil, Nikon Corp, Tokyo, Japan). The emission beam is imaged through a 50 μm diameter pinhole and split onto two spectrally filtered single photon avalanche diode (SPAD) detectors (Micro Photon Devices) as described previously [27]. Measurements were performed at 37 °C by a stage-top incubator (Chamlide IC, QuorumTechnologies, Guelph, Ontario, Canada). The laser powers were set to 1 μW for the blue (488 nm) laser and 1 μW for the green (561 nm) laser before the measurements. For each area of SLB analyzed, the data were collected in 15 sets of 15 s acquisitions by a time-correlated single photon counting (TCSPC) device (Picoharp300, PicoQuant, Berlin, Germany). Each data point reported in the figures is the average of five different areas obtained from at least three individual SLBs.

The autocorrelation function data were fit with a simple 2D diffusion model:

$$G(\tau) = \frac{1}{\langle N \rangle}\left[1 + \frac{\tau}{\tau_D}\right]^{-1}, \tag{1}$$

where N is the average number of diffusing species and τ_D is the dwell time of fluorescence particles in the detection area.

The autocorrelation function data were also fitted with a two-component diffusion model, which allowed us to determine the diffusion of free and bound species separately. The two-component diffusion model is defined as,

$$G_{2D}(\tau) = \frac{1}{\langle N \rangle}\left[(1-y)\left[1 + \frac{\tau}{\tau_{D1}}\right]^{-1} + y\left[1 + \frac{\tau}{\tau_{D2}}\right]^{-1}\right]. \tag{2}$$

Here, N is the average number of fluorescent molecules in the detection area, τ_{D1} and τ_{D2} are the dwell time of fast and slow species, respectively and y is the fraction of molecules diffusing at τ_{D2}. The diffusion coefficient D, is defined by the relationship

$$\tau_D = \frac{\omega_0^2}{4D}, \tag{3}$$

where ω_0 is the radius of the detection area. From this equation, we calculate the diffusion coefficients of the fast species, D_1, and slow species, D_2.

The degree of lipid-peptide binding is quantified with the parameter f_c, which ranges from 0 to 1, depending on how many particles co-diffuse through the detection area:

$$f_c = \frac{Nrg}{\min[(Nr + Nrg), (Ng + Nrg)]}. \quad (4)$$

Fluorescence lifetime is reported as τ_{fl}, which is calculate by a single-exponential fit

$$F(t) = e^{-t/\tau_{fl}}. \quad (5)$$

3. Results

3.1 Bilayer preparation and peptide binding assays

We first created a supported lipid bilayer (SLB) with nickel-chelating lipids and fluorescent PIP_2 asymmetrically distributed into the upper leaflet of the bilayer [22]. Nickel-chelating lipids were used to anchor histidine-tagged peptides to the plasma membrane similar to previous SLB assays [28]. PIP_2 lipids were purchased from Avanti Polar Lipids, which contain a BODIPY analogue, TopFluor attached to the acyl chain of $PI(4,5)P_2$ (TF-PIP_2). Two buffers were prepared, buffer **A**, which has a relatively low ionic strength (10x dilution of PBS) and buffer **B**, which has a higher ionic strength buffer (undiluted, 1x PBS, see Materials and Methods). Preparation of SLBs was done by vesicle rupture fusion with SUVs containing DOPC and DOGS-NTA-Ni^{2+}(96.5:3.5) deposited on a hydrophilic glass surface. After bilayer formation, buffer A was used to wash the lipid bilayers. Next, a DOPC, DOPS and TF-PIP_2 (94.95:5:0.05) lipid film was hydrated by adding 1 mL of water. A small aliquot of these hydrated liposomes was added to the buffer above the SLBs, which led to incorporation of TF-PIP_2 into the top leaflet as described previously [22]. Buffer A was again used to wash the system before measurement. The precise concentration of TF-PIP_2 was measured with FCS, and the micron-scale mobility of PIP_2 lipids was verified with fluorescence recovery after photobleaching (FRAP).

Polycationic peptides His_8-Lys_8 and His_8-$MARCKS_{(152-176)}$ were synthesized and labeled with red fluorescent dye 5-carboxytetramethylrhodamine (TAMRA) as described in the Materials and Methods. The peptide

sequences and the lipid chemical structures are shown in Fig. 1. Binding of the peptides to the model membranes was monitored by epi-fluorescence imaging and FRAP experiments. Upon adsorption of peptides to the asy-SLBs, epi-fluorescence imaging shows a homogeneous distribution of TF-PIP_2 and His_8-Lys_8 (Fig. 6A and B, left) or TF-PIP_2 and His_8-$MARCKS_{(152-176)}$ (Fig. 6C and D, left). FRAP experiments on the peptide-adsorbed asy-SLBs showed 100% fluorescence intensity recovery within 30s for both fluorescent probes, which indicates that the lipids and peptides are highly mobile after peptide binding (Fig. 6E). The concentration and mobility of the peptides and lipids were quantified with FCS as described in the following section.

3.2 Dual-color PIE-FCCS measures the interaction of polybasic peptides with TF-PIP_2 lipids

To characterize the diffusion dynamics of lipids and peptides, we first discuss the single color FCS data in Fig. 2A and 2B. Fig. 2A is the autocorrelation

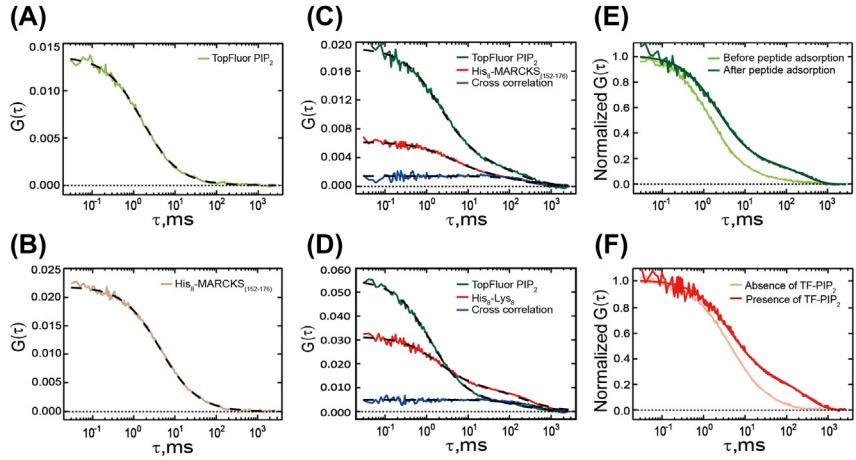

Figure 2 FCS data is shown for (A) TF-PIP_2 in asy-SLBs and (B) His_8-$MARCKS_{(152-176)}$ adsorbed on SLBs without TF-PIP_2 lipid. Panels (C—D) show the PIE-FCCS data of asy-SLBs containing TF-PIP_2 and bound His_8-$MARCKS_{(152-176)}$ (C) and TF-PIP_2 with bound His_8-Lys_8 (D). The autocorrelation functions for TF-PIP_2 are shown in green; His-tagged peptides are shown in red; and the cross-correlation functions are shown in blue. Panel (E) shows the normalized autocorrelation curves of TF-PIP_2 before (light green) and after (dark green) His_8-$MARCKS_{(152-176)}$ adsorption for the same bilayer. Panel (F) shows the normalized autocorrelation curves of His_8-$MARCKS_{(152-176)}$ adsorbed on lipid bilayer with (dark red) or without (light red) TF-PIP_2 lipids. All data are under low ionic strength buffer **A**. In all the curves, black dashed lines are two-component diffusion model fits to the data.

function corresponding to TF-PIP_2 in an asy-SLB with no peptide. Fig. 2B is the autocorrelation function of His_8-$MARCKS_{(152-176)}$ peptide adsorbed to an SLBs with no TF-PIP_2. Both sets of data fit well to a simple 2D diffusion model (Eq. 1), which yielded an average dwell time (τ_D) of 1.46 ms (TF-PIP_2) and 3.78 ms (His_8-$MARCKS_{(152-176)}$).

To quantify the interactions of TF-PIP_2 with His_8-$MARCKS_{(152-176)}$ we used two-color, PIE-FCCS [29]. This method simultaneously recorded single color FCS data for both the lipid and peptide. It also generated a cross-correlation function, in which the amplitude reports on correlated fluctuations of the lipid and peptide. The PIE-FCCS data for peptides bound to a TF-PIP_2-containing asy-SLB (Fig. 2C and D) showed a significant level of cross-correlation for both His_8-$MARCKS_{(152-176)}$ and His_8-Lys_8. To quantify the degree of cross-correlation we calculate the ratio of the auto- and cross-correlation functions at early times, represented by the variable, f_c, as described in the Materials and Methods section [30]. The value of f_c ranges from 0 to 1 and will increase with the number of lipid-peptide complexes formed [20] As reported in Fig. 3, the average f_c value for His_8-$MARCKS_{(152-176)}$ with TF-PIP_2 at low ionic strength buffer (buffer A) is 0.103 ± 0.03, indicating significant interactions between the MARCKS peptides and PIP_2 lipids. The data for His_8-Lys_8 and TF-PIP_2 in buffer A reveals a similar result (0.133 ± 0.04). The f_c value for

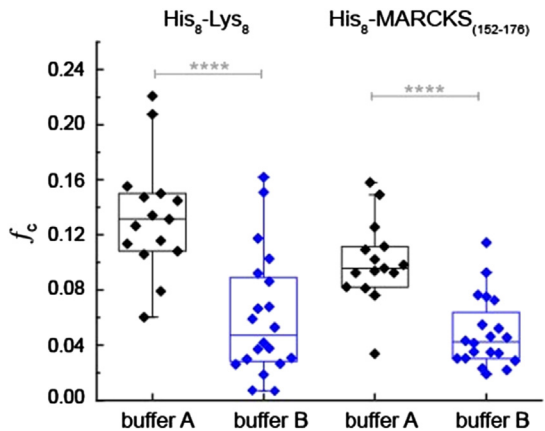

Figure 3 Summary of the f_c values measured for several bilayers containing His_8-Lys_8: TF-PIP_2 and His_8-$MARCKS_{(152-176)}$:TF-PIP_2 under different buffer conditions. Low ionic strength buffer **A** is plotted in black and high ionic strength buffer **B** is in blue. The line in the center of each box is the median of the distribution. One-way ANOVA tests were performed to determine p-values (**** indicates $p < 0.0001$).

His_8-$MARCKS_{(152-176)}$ and His_8-Lys_8 with TF-PIP_2 indicated the presence of strong binding and stable complexation between the peptides and lipids. In addition, binding between His_8-Lys_8 and TF-PIP_2 were observed to be slightly higher than His_8-$MARCKS_{(152-176)}$.

Electrostatic forces are assumed to be the driving force in these lipid-peptide interactions. Thus, the correlated diffusion we observed with PIE-FCCS is likely to be influenced by the surrounding salt concentration through classic Debye-Hückel screening [31]. To confirm this idea, we measure the average f_c value of His_8-$MARCKS_{(152-176)}$ (0.048 ± 0.03) and His_8-Lys_8 (0.061 ± 0.04) with TF-PIP_2 at high ionic strength buffer (buffer B). These values are significantly lower than we observed at lower ionic strength (buffer A) for His_8-$MARCKS_{(152-176)}$ (0.103 ± 0.03) and His_8-Lys_8 (0.133 ± 0.04).

We also conducted experiments with TF-labeled phosphatidylserine (TF-PS), a lipid with a formal charge of -1 compared to -3 for PIP_2 [32]. Sample FCS data for TF-PS and His_8-$MARCKS_{(152-176)}$ before and after binding are shown in Fig. 4. We observed significant cross-correlation between TF-PS lipids upon the peptide binding, consistent with PIP_2 lipid results. The degree of cross-correlation, however was slightly reduced, the average f_c value for TF-PS and His_8-$MARCKS_{(152-176)}$ was 0.076 ± 0.02 compared to 0.103 ± 0.03 for TF-PIP_2 and His_8-$MARCKS_{(152-176)}$ under the low ionic strength buffer. These data show the expected result of lower binding between cationic peptides and PS compared to PIP_2, and are further evidence that the interactions between these peptides and PIP_2 is driven primarily by electrostatic interactions.

3.3 Two component diffusion

Another salient feature of the PIE-FCCS data is the appearance of a long lag time component at $\tau \sim 300$ ms, which is seen in both the lipid and peptide autocorrelation functions. This long lag time component is only visible when both labeled components (His_8-$MARCKS_{(152-176)}$ and TF-PIP_2) are present in the membrane. To illustrate this point, the FCS data before and after binding are shown in Fig. 2E and F. In Fig. 2E, TF-PIP_2 autocorrelation data is shown for the same bilayer before and after peptide binding. In Fig. 2F, peptide autocorrelation data is shown for bilayers with and without TF-PIP_2. For both the lipid and the peptide autocorrelation data, the second time-component arises only when both species are present.

In order to be interpret this long-time component, we fit the FCS data to a 2D, two-component diffusion model (Eq. 2), the fast species (τ_{D1}) is

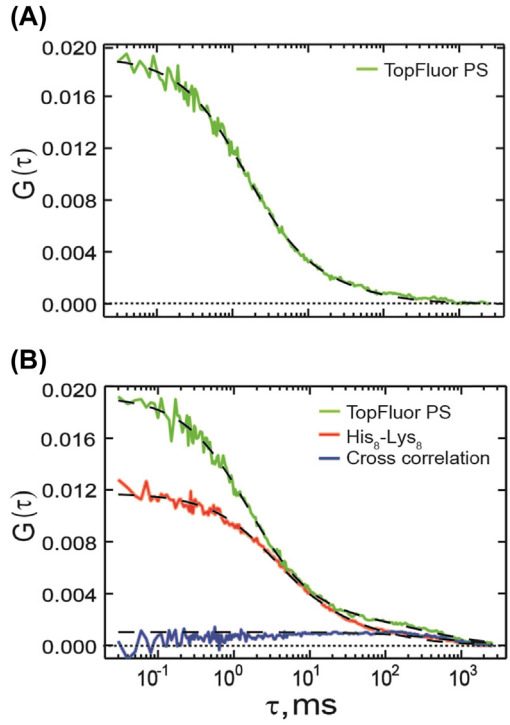

Figure 4 The autocorrelation curve of TF-PS lipid (A) before and (B) after His_8-$MARCKS_{(152-176)}$ adsorption. The autocorrelation function for TF-PS are shown in green, for his-tagged peptides are shown in red, and the cross-correlation function for the lipid-peptide complexes are shown in blue. The *black dished line* is representing the zero value for compare with the cross-correlation function.

interpreted as free lipids and peptides, while the slow species (τ_{D2}) is interpreted as bound lipids and peptide complexes [25]. This model is used to fit the autocorrelation functions. The cross-correlation function is fit with the 2D, single component model, G(τ), and the amplitude is proportional to the co-diffusion of the two labeled species [33]. With this two-component diffusion model we analyzed the dwell times, τ_{D1} and τ_{D2}, to determine their respective diffusion coefficients. Because there are two labeled species, we analyzed the diffusion coefficient of peptide and lipid separately. As reported in Table 1, focusing on the lipids first, we observed that TF-PIP_2 before peptide adsorption had an average diffusion coefficient of 6.78 $\mu m^2/s$ at (Fig. 5A, buffer A). Upon His_8-$MARCKS_{(152-176)}$ adsorption, the diffusion coefficient corresponding to the fast component is 7.13 $\mu m^2/s$. This observation suggests that the diffusion coefficient of fast lipid

Table 1 Summary of PIE-FCCS data with two-component diffusion model.

	f_c (mean)[c]	$D_{G,O}$ ($\mu m^2/s$)[d]	$D_{G,F}$ ($\mu m^2/s$)[d]	$D_{G,S}$ ($\mu m^2/s$)[d]	$D_{R,F}$ ($\mu m^2/s$)[d]	$D_{R,S}$ ($\mu m^2/s$)[d]
His-Lys[a]	0.133 ± 0.04	8.517 ± 0.33	8.213 ± 0.29	0.086 ± 0.01	5.755 ± 0.32	0.151 ± 0.03
His-MARCKS[a]	0.103 ± 0.03	6.780 ± 0.10	7.131 ± 0.34	0.311 ± 0.09	4.088 ± 0.33	0.153 ± 0.03
His-Lys[b]	0.061 ± 0.05	7.610 ± 0.25	8.194 ± 0.11	0.198 ± 0.07	5.548 ± 0.22	0.390 ± 0.11
His-MARCKS[b]	0.049 ± 0.03	7.139 ± 0.09	7.482 ± 0.10	0.151 ± 0.03	4.792 ± 0.21	0.930 ± 0.11

[a]Data are reported from experiments in buffer **A**.
[b]Data are reported from experiments in buffer **B**.
[c]Fraction correlate, f_c is calculated from two-component diffusion fit and shown in Fig. 3. Values are reported as the mean ± SD.
[d]$D_{G,O}$, $D_{G,F}$, $D_{G,S}$, $D_{R,F}$ and $D_{R,S}$ are the original diffusion coefficient of PIP_2 lipid before peptide adsorption, fast and slow diffusion coefficient of PIP_2 lipid after peptide adsorption, fast and slow diffusion coefficient of peptide, respectively; These values are form Fig. 5 and represented as the mean ± SE.

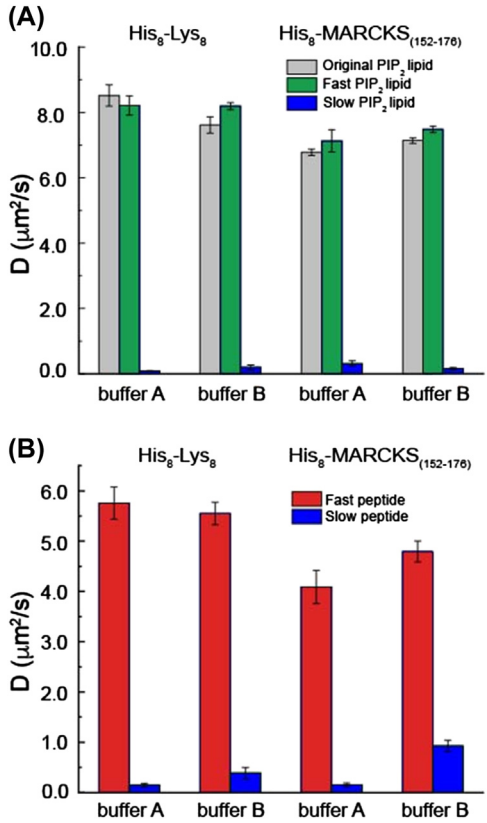

Figure 5 (A) Fast and slow diffusion coefficients of TF-PIP_2 lipids calculated from the two-component diffusion fit. The *gray bar* represents the diffusion coefficients of TF-PIP_2 before peptide binding, while the green bar represents the fast diffusion coefficient after peptide binding. The blue bar is the slow diffusion coefficient of TF-PIP_2 after peptide binding. (B) Fast and slow diffusion coefficients of peptides are calculated from the two-component diffusion fit. *Red bars* represent the fast diffusion coefficient; *blue bars* represent the slow diffusion coefficient.

component is very similar to the diffusion coefficient before peptide binding, as expected for lipids that do not associate with the peptides. The diffusion coefficient of the long lag-time component is 0.31 $\mu m^2/s$, which is more than 23 times slower than diffusion coefficient of fast component and is consistent with the theory that the formation of peptide-lipid complexes will reduced mobility. For the peptide autocorrelation data, two-component diffusion analysis of His_8-$MARCKS_{(152-176)}$ associate with the model membrane yielded an averaged diffusion coefficient of 4.09 $\mu m^2/s$ for the fast component and 0.15 $\mu m^2/s$ for the slow component

(Fig. 5B). Similar to the lipid diffusion data, the diffusion coefficient of the peptide slow component is 27 times slower than the fast component. The mobility data for TF-PIP_2 with His_8-Lys_8 is consistent with results for the MARCKS peptide (Fig. 5A and B).

The effects of buffer on the diffusion coefficient were also measured for peptides and lipids. Despite some variation between bilayers, diffusion of the lipid species does not show any significant change when comparing mobility data from buffer A to that from buffer B (Fig. 5A). For the peptide, we note that there is an increase of the slow diffusion component in buffer B for both Lys and MARCKS peptide (Fig. 5B).

Under the interpretation that the long lag-time component of the autocorrelation data corresponds to a lipid-peptide complex, we can estimate the size of the complex using a model for two-dimensional diffusion in the membrane. The Saffman–Delbrück model has been successfully applied to deal with a range of protein complexes in a 2D system [34]. Using this model, we calculate the radius of the slow-moving complexes with the following equation:

$$r_{slow} = r_{fast} \cdot exp\left[\left(1 - \frac{D_{slow}}{D_{fast}}\right) \cdot \left(\ln\left(\frac{\mu_m \cdot h}{\mu_w \cdot r_{fast}}\right) - 0.5772\right)\right]$$

As an example, the radius of the complex, r_{slow}, calculated from the lipid data is 190 *nm* in buffer A (assuming $r_{fast} = 0.14\ nm$; $\mu_m = 2.94\ P$; $\mu_w = 0.01\ P$; *and* $h = 1.6\ nm$). Using the peptide data, the radius of the complex is 200 nm, consistent with the lipid results. These calculated sizes are quite large, implying that such complexes would be visible as bright punctate features in the fluorescence images of the bilayer. To illustrate the calculation of peptide-lipid complexes radius is correct, we provided the time-average fluorescence images of lipid (Fig. 6A and C, right) and peptide (Fig. 6B and D, right). The bright punctate spots were observed in the fluorescence images for both His_8-Lys_8 and His_8-$MARCKS_{(152\text{-}176)}$ interactions. This means that the scaling of the diffusion coefficient with the radius is affected by lipid-peptide interactions and the long lag-time component correspond to the large-size lipid-peptide complexes. One complication to these estimates is that theories for scaling of the diffusion coefficient for membrane complexes are still being developed. Details like coupling to the bilayer, microscopic defects, and the kinetics of lipid-peptide coupling could strongly affect the accuracy of the size estimate. In the next section, we investigate photophysical changes that could result from the close association of fluorescent labels in these complexes, which could also affect the size estimate.

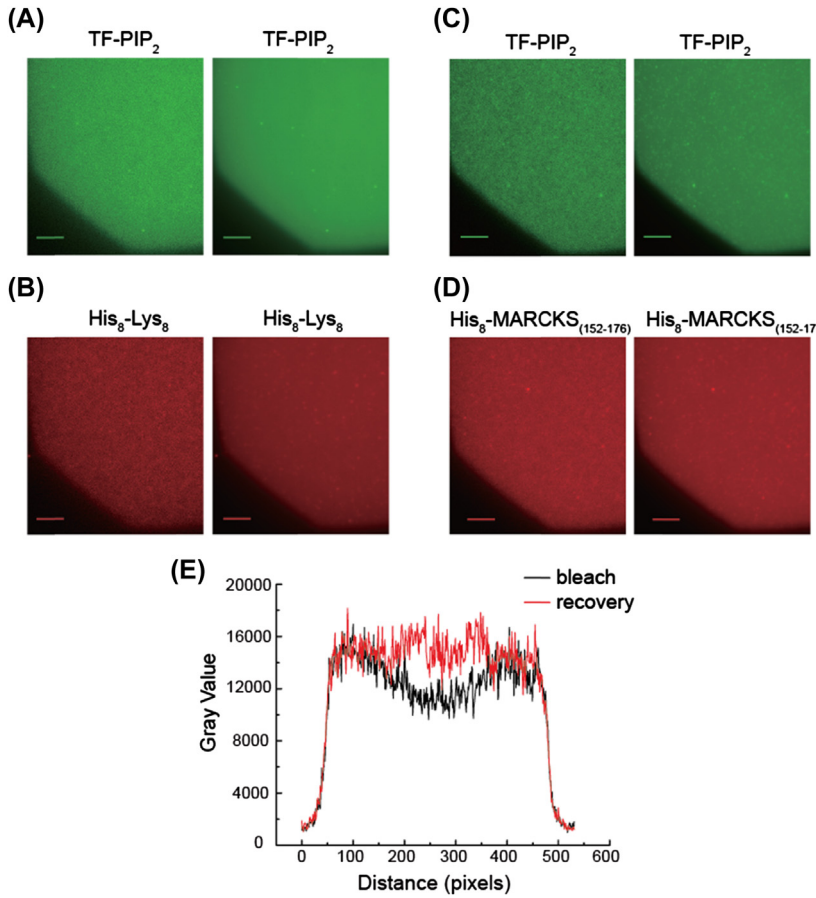

Figure 6 (A) Epi-fluorescence images (left) and time-averaged images (right) of asymmetric SLB containing 0.05% TF-PIP_2 and (B) adsorbed His_8-Lys_8. (C) Epi-fluorescence images (left) and time-averaged images (right) of asymmetric SLB containing 0.05% TF-PIP_2 and (D) adsorbed His_8-$MARCKS_{(152-176)}$. The scale bars are 5 μm. The bright punctate particles observed form time-average images indicates that large-sized lipid-peptide complexes was formed. (E) Fluorescence recovery after photobleaching (FRAP) curves of His_8-$MARCKS_{(152-176)}$ peptides adsorbed TF-PIP_2 asy-SLB. The *red line* is represented recovery of TF-PIP_2 lipid and the bleach data are shown in black.

3.4 Photophysical changes upon peptide binding

Lipid-peptide associations could lead to static quenching and energy transfer because of the proximity of the fluorescent probes [35,36]. If present, these photophysical changes will be reflected in the fluorescence lifetime

Table 2 Overview of molecular brightness (η) and fluorescence lifetime (τ_{fl}) data.

	His-Lys[c]	Original bilayer[c]	His-MARCKS[c]	Original bilayer[c]
η_G (cpms)[a]	799 ± 29	1277 ± 73	554 ± 64	1330 ± 54
τ_{fl} (ns)[b]	4.205 ± 0.18	4.682 ± 0.06	4.109 ± 0.33	4.633 ± 0.02

Original bilayer is the data calculated from the bilayer before peptide adsorption.
[a]η_G, Molecular brightness and data are represented as the mean ± SE.
[b]τ_{fl}, fluorescence lifetime and data are represented as the mean ± SE.
[c]Data are reported from experiments in buffer **A** and displayed in Fig. 7.

and molecular brightness of the fluorophores. Fluorescence lifetimes were extracted from lifetime histograms constructed with the same time-correlated single photon counting data collected for PIE-FCCS measurements. Molecular brightness and lifetime data are reported in Table 2. Fluorescence lifetime, τ_{fl}, is calculated by single-exponential fits to the lifetime histograms (see Materials and Methods) [37]. As shown in Fig. 7A, the average lifetime of TF-PIP_2 upon the His_8-Lys_8 adsorption decreased from 4.68 ± 0.06 ns to 4.01 ± 0.18 ns. The average lifetime of TF-PIP_2 upon adsorption of His_8-$MARCKS_{(152-176)}$ decreased from 4.63 ± 0.02 ns to 4.11 ± 0.33 ns. This decrease in the lifetime for both lipid-peptide systems suggests that there are significant quenching events upon peptide binding. Molecular brightness values before and after peptide adsorption are consistent with this conclusion (Fig. 7B). The molecular brightness of TF-PIP_2 upon adsorption of His_8-Lys_8 decreased 37.5% (from 1277 ± 73 cpsm to 799 ± 29 cpsm). Under the same conditions, the molecular brightness of TF-PIP_2 upon adsorption of His_8-$MARCKS_{(152-176)}$ decreased 58.3% (from 1330 ± 54 cpsm to 554 ± 64 cpsm). Together, the lifetime and molecular brightness data show that the environment of the TF fluorescent probe changes significantly upon peptide binding. These photophysical changes are consistent with tight binding of the lipid and peptide, and make it impossible to extract precise estimates for the number of lipids and peptides per complex.

4. Discussion

With our time-resolved fluorescence approach, we quantified binding of polycationic peptides to anionic lipids in model supported lipid bilayers. We observed cross-correlation between the lipid and peptide probes indicating specific, long-lived interactions. The cross-correlation decreased

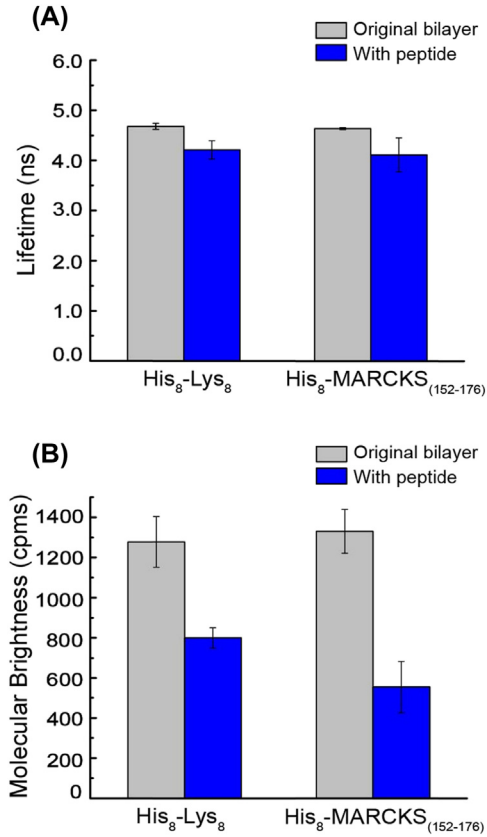

Figure 7 Lifetime (A) and molecular brightness (B) data for TF-PIP_2 asy-SLBs before and after adding His_8-Lys_8 and His_8-$MARCKS_{(152-176)}$ in low ionic buffer condition (buffer **A**). Gray bar is before peptide adsorption, and the blue bar is after peptide adsorption.

when going from low to high ionic strength buffer conditions and when comparing the less negatively charged TF-PS lipids to TF-PIP_2. These data indicate that lipid-peptide binding is driven by electrostatic attractions between negatively charged lipids and positively charged amino acid side chains on the peptides. More importantly, these data establish that stable lipid-peptide complexes diffuse as individual species. While much of the parameter space still needs to be explored, data like that presented above provide unique experimental evidence for the stability of lipid-peptide complexes under specific environmental conditions. The idea of using FCCS to measure lipid-protein interactions has been mentioned in previous reviews [25,29]. However, experimental evidence of cross-correlation between lipid

and any peptide or protein system has not been reported. The experimental approach described here opens new routes to determining the binding affinity between lipids and proteins.

The autocorrelation curves upon peptide binding showed a surprising long lag-time component. We used a two-component diffusion model, which assumes that the system partitions into fast and slow diffusion states. The fast-moving species are assigned as free (unbound) lipids and peptides. The slow-moving species are assigned to bound lipid-peptide complexes, which are less mobile due to increased friction with the membrane. Based on this assumption, the two-component diffusion model measures fast and slow diffusion for both peptide and lipid as well as the mobility of the lipid-peptide complexes.

In this paper we have shown that PIE-FCCS is a powerful tool for resolving lipid-peptide interactions. Such interactions are at the heart of information transfer across the plasma membrane and are essential to understanding cell signaling. This work will enable future investigations of lipid interactions with functional protein domains, which one could then determine hot spot residues for lipid binding.

Acknowledgements

Research reported in this publication was supported by the National Science Foundation under grant number CHE-1753060 and the National Eye Institute of the National Institutes of Health under award number R15EY024451.

References

[1] A. Gambhir, G. Hangyas-Mihalyne, I. Zaitseva, D.S. Cafiso, J. Wang, D. Murray, S.N. Pentyala, S.O. Smith, S. McLaughlin, Electrostatic sequestration of PIP2 on phospholipid membranes by basic/aromatic regions of proteins, Biophys. J. 86 (4) (2004) 2188–2207.

[2] S. McLaughlin, D. Murray, Plasma membrane phosphoinositide organization by protein electrostatics, Nature 438 (7068) (2005) 605–611.

[3] M. Liscovitch, V. Chalifa, P. Pertile, C.S. Chen, L.C. Cantley, Novel function of phosphatidylinositol 4,5-bisphosphate as a cofactor for brain membrane phospholipase D, J. Biol. Chem. 269 (34) (1994) 21403–21406.

[4] S.B. Hansen, X. Tao, R. MacKinnon, Structural basis of PIP2 activation of the classical inward rectifier K+ channel Kir2.2, Nature 477 (7365) (2011) 495–498.

[5] O. Cremona, G. Di Paolo, M.R. Wenk, A. Luthi, W.T. Kim, K. Takei, L. Daniell, Y. Nemoto, S.B. Shears, R.A. Flavell, D.A. McCormick, P. De Camilli, Essential role of phosphoinositide metabolism in synaptic vesicle recycling, Cell 99 (2) (1999) 179–188.

[6] J.B. Seo, S.R. Jung, W. Huang, Q. Zhang, D.S. Koh, Charge Shielding of PIP2 by Cations Regulates Enzyme Activity of Phospholipase C, PLoS One 10 (12) (2015) p. e0144432.

[7] A. Anderluh, T. Hofmaier, E. Klotzsch, O. Kudlacek, T. Stockner, H.H. Sitte, G.J. Schutz, Direct PIP2 binding mediates stable oligomer formation of the serotonin transporter, Nat. Commun. 8 (2017) 14089.
[8] H. Jung, A.D. Robison, P.S. Cremer, Multivalent ligand-receptor binding on supported lipid bilayers, J. Struct. Biol. 168 (1) (2009) 90–94.
[9] J. Wang, A. Arbuzova, G. Hangyas-Mihalyne, S. McLaughlin, The effector domain of myristoylated alanine-rich C kinase substrate binds strongly to phosphatidylinositol 4,5-bisphosphate, J. Biol. Chem. 276 (7) (2001) 5012–5019.
[10] B.P. Ziemba, J.E. Burke, G. Masson, R.L. Williams, J.J. Falke, Regulation of PI3K by PKC and MARCKS: single-molecule analysis of a reconstituted signaling pathway, Biophys. J. 110 (8) (2016) 1811–1825.
[11] L.A. Morton, R. Tamura, A.J. de Jesus, A. Espinoza, H. Yin, Biophysical investigations with MARCKS-ED: dissecting the molecular mechanism of its curvature sensing behaviors, Biochim. Biophys. Acta 1838 (12) (2014) 3137–3144.
[12] J.F. Ellena, M.C. Burnitz, D.S. Cafiso, Location of the myristoylated alanine-rich C-kinase substrate (MARCKS) effector domain in negatively charged phospholipid bicelles, Biophys. J. 85 (4) (2003) 2442–2448.
[13] U. Dietrich, P. Kruger, T. Gutberlet, J.A. Kas, Interaction of the MARCKS peptide with PIP2 in phospholipid monolayers, Biochim. Biophys. Acta 1788 (7) (2009) 1474–1481.
[14] L. Rusu, A. Gambhir, S. McLaughlin, J. Radler, Fluorescence correlation spectroscopy studies of Peptide and protein binding to phospholipid vesicles, Biophys. J. 87 (2) (2004) 1044–1053.
[15] J. Korlach, P. Schwille, W.W. Webb, G.W. Feigenson, Characterization of lipid bilayer phases by confocal microscopy and fluorescence correlation spectroscopy, Proc. Natl. Acad. Sci. U. S. A. 96 (15) (1999) 8461–8466.
[16] K. Bacia, P. Schwille, Practical guidelines for dual-color fluorescence cross-correlation spectroscopy, Nat. Protoc. 2 (11) (2007) 2842–2856.
[17] P. Schwille, F.J. Meyer-Almes, R. Rigler, Dual-color fluorescence cross-correlation spectroscopy for multicomponent diffusional analysis in solution, Biophys. J. 72 (4) (1997) 1878–1886.
[18] K. Bacia, S.A. Kim, P. Schwille, Fluorescence cross-correlation spectroscopy in living cells, Nat. Methods 3 (2) (2006) 83–89.
[19] M. Marita, Y. Wang, M.J. Kaliszewski, K.C. Skinner, W.D. Comar, X. Shi, P. Dasari, X. Zhang, A.W. Smith, Class A plexins are organized as preformed inactive dimers on the cell surface, Biophys. J. 109 (9) (2015) 1937–1945.
[20] X. Shi, X. Li, M.J. Kaliszewski, X. Zhuang, A.W. Smith, Tuning the mobility coupling of quaternized polyvinylpyridine and anionic phospholipids in supported lipid bilayers, Langmuir 31 (5) (2015) 1784–1791.
[21] B.K. Muller, E. Zaychikov, C. Brauchle, D.C. Lamb, Pulsed interleaved excitation, Biophys. J. 89 (5) (2005) 3508–3522.
[22] X. Shi, M. Kohram, X. Zhuang, A.W. Smith, Interactions and translational dynamics of phosphatidylinositol bisphosphate (PIP2) lipids in asymmetric lipid bilayers, Langmuir 32 (7) (2016) 1732–1741.
[23] L.A. Morton, H. Yang, J.P. Saludes, Z. Fiorini, L. Beninson, E.R. Chapman, M. Fleshner, D. Xue, H. Yin, MARCKS-ED peptide as a curvature and lipid sensor, ACS Chem. Biol. 8 (1) (2013) 218–225.
[24] J.A. Nye, J.T. Groves, Kinetic control of histidine-tagged protein surface density on supported lipid bilayers, Langmuir 24 (8) (2008) 4145–4149.
[25] A.J. Garcia-Saez, P. Schwille, Fluorescence correlation spectroscopy for the study of membrane dynamics and protein/lipid interactions, Methods 46 (2) (2008) 116–122.

[26] Q. Wang, G. Liang, M. Zhang, J. Zhao, K. Patel, X. Yu, C. Zhao, B. Ding, G. Zhang, F. Zhou, J. Zheng, De novo design of self-assembled hexapeptides as beta-amyloid (Abeta) peptide inhibitors, ACS Chem. Neurosci. 5 (10) (2014) 972–981.
[27] W.D. Comar, S.M. Schubert, B. Jastrzebska, K. Palczewski, A.W. Smith, Time-resolved fluorescence spectroscopy measures clustering and mobility of a G protein-coupled receptor opsin in live cell membranes, J. Am. Chem. Soc. 136 (23) (2014) 8342–8349.
[28] H. Nakashima, K. Furukawa, Y. Kashimura, K. Sumitomo, Y. Shinozaki, K. Torimitsu, Pattern formation and molecular transport of histidine-tagged GFPs using supported lipid bilayers, Langmuir 26 (15) (2010) 12716–12721.
[29] A.W. Smith, Lipid-protein interactions in biological membranes: a dynamic perspective, Biochim. Biophys. Acta 1818 (2) (2012) 172–177.
[30] N.F. Endres, R. Das, A.W. Smith, A. Arkhipov, E. Kovacs, Y. Huang, J.G. Pelton, Y. Shan, D.E. Shaw, D.E. Wemmer, J.T. Groves, J. Kuriyan, Conformational coupling across the plasma membrane in activation of the EGF receptor, Cell 152 (3) (2013) 543–556.
[31] M.E. Fisher, Y. Levin, Criticality in ionic fluids: Debye-Huckel theory, Bjerrum, and beyond, Phys. Rev. Lett. 71 (23) (1993) 3826–3829.
[32] J. Kim, T. Shishido, X. Jiang, A. Aderem, S. McLaughlin, Phosphorylation, high ionic strength, and calmodulin reverse the binding of MARCKS to phospholipid vesicles, J. Biol. Chem. 269 (45) (1994) 28214–28219.
[33] P. Schwille, J. Bieschke, F. Oehlenschlager, Kinetic investigations by fluorescence correlation spectroscopy: the analytical and diagnostic potential of diffusion studies, Biophys. Chem. 66 (2–3) (1997) 211–228.
[34] P.G. Saffman, M. Delbruck, Brownian motion in biological membranes, Proc. Natl. Acad. Sci. U. S. A. 72 (8) (1975) 3111–3113.
[35] V.V. Didenko, DNA probes using fluorescence resonance energy transfer (FRET): designs and applications, Biotechniques 31 (5) (2001), p. 1106–1116, 1118, 1120–1121.
[36] L.A. Munishkina, A.L. Fink, Fluorescence as a method to reveal structures and membrane-interactions of amyloidogenic proteins, Biochim. Biophys. Acta 1768 (8) (2007) 1862–1885.
[37] W. Becker, Advanced Time-Correlated Single Photon Counting Techniques, in: Springer Series in Chemical Physics, xix, Springer, Berlin; New York, 2005, 401 p.